Robust Lateral Control of long-combination vehicles under Moments of Inertia and Tire Cornering Stiffness Uncertainties

Taylor & Francis
Taylor & Francis Group

Vehicle System Dynamics
International Journal of Vehicle Mechanics and Mobility

ISSN: 0042-3114 (Print) 1744-5159 (Online) Journal homepage: https://www.tandfonline.com/loi/nvsd20

Robust lateral control of long-combination vehicles under moments of inertia and tyre cornering stiffness uncertainties

Maliheh Sadeghi Kati, Hakan Köroğlu & Jonas Fredriksson

To cite this article: Maliheh Sadeghi Kati, Hakan Köroğlu & Jonas Fredriksson (2019) Robust lateral control of long-combination vehicles under moments of inertia and tyre cornering stiffness uncertainties, Vehicle System Dynamics, 57:12, 1847-1873, DOI: 10.1080/00423114.2018.1552363

To link to this article: https://doi.org/10.1080/00423114.2018.1552363

Published online: 09 Dec 2018.

VEHICLE SYSTEM DYNAMICS
2019, VOL. 57, NO. 12, 1847–1873
https://doi.org/10.1080/00423114.2018.1552363

Robust lateral control of long-combination vehicles under moments of inertia and tyre cornering stiffness uncertainties

Maliheh Sadeghi Kati, Hakan Köroğlu and Jonas Fredriksson

Division of Systems and Control, Department of Electrical Engineering, Chalmers University of Technology, Gothenburg, Sweden

ABSTRACT

A robust steering-based controller synthesis is presented for an A-double combination vehicle with a steerable dolly. The controller ensures robust stability and performance in the face of uncertainties in the cornering stiffness of the tyres and the moments of inertia of the semitrailers, which are treated as time-varying and time-invariant parameters respectively. A descriptor-type representation of the system is employed since a standard state-space model depends rationally on the moments of inertia. The controller synthesis is formulated as an $\mathscr{H}_\infty$-type static output feedback, which uses information from only one articulation angle. The driver steering input is also used by including a static feed-forward. The proposed synthesis method is based on linear matrix inequality (LMI) optimisation. The controller is verified based on the simulation results obtained from both (approximate) linear and (high-fidelity) nonlinear vehicle models. The results indicate significant improvement in the high-speed lateral performance of the A-double in the presence of parametric uncertainties.

ARTICLE HISTORY
Received 1 June 2018
Revised 22 October 2018
Accepted 19 November 2018

KEYWORDS
Robust lateral control; static output feedback; active dolly; rearward amplification and parametric uncertainty

1. Introduction

Lateral control of long-combination vehicles for low and high speeds has long been an active research area. The majority of the lateral control approaches for long-combination vehicles (e.g. [1–6]) are based on the assumption that parameters and variables of the considered vehicle model for control designs are known and measurable or can be estimated. Consequently, the applicability of the control systems are restricted by the accuracy of vehicle parameters such as yaw moment of inertia, mass, location of center of gravity and tyre cornering stiffness coefficients.

However, new technologies such as on-board weighing (OBW) or weigh-in-motion (WIM) [7,8] make it possible to measure and monitor the axle load as well as the total mass and consequently estimate the centre of gravity of each vehicle unit. On the other hand, the moment of inertia of the vehicle units and the cornering stiffness of the tyres are inevitably the most uncertain vehicle parameters that are difficult or impossible to be accurately measured or estimated. These parameters may vary depending on many factors

CONTACT Maliheh Sadeghi Kati kani@chalmers.se

such as the variety of possible loading conditions, variation of tyre inflating pressure, road surface condition, weather condition, etc. Therefore, there is a crucial need to design the controller in such a way that the controlled vehicle not only maintains robust stability in the presence of parameter uncertainties and un-modelled dynamics but also achieves a desirable level of robust performance. This approach of design in the presence of parametric uncertainty, called robust control, requires no information about the uncertain parameters besides the knowledge of their minimum and maximum values and also lower and upper bounds on the rates-of-variation of time-varying parameters. Only a few works in the literature suggest robust syntheses for heavy-duty vehicles (e.g. [9–15]) considering robustness against uncertainties in the vehicle parameters such as the vehicle longitudinal speed, road adhesion coefficient, cargo loads in trailers, the tyre cornering stiffness and actuator model uncertainty. To the best of our knowledge, no existing research on heavy vehicles has addressed robust syntheses to deal simultaneously with uncertainties in both tyre cornering stiffness and yaw moment of inertia.

In this paper, the design of a robust lateral controller is considered for an A-double combination vehicle (tractor-semitrailer-dolly-semitrailer) equipped with an active dolly steering system as shown in Figure 1(a). The main objective of the controller is to guarantee robust stability and improve the lateral performance of the vehicle at high speeds in the face of parametric uncertainties such as the cornering stiffness of the tyres and the yaw moments of inertia of the semitrailers. The controller design problem is formulated based on a static output feedback synthesis in which only one easily measurable state variable is required. As the measurement of the driver steering is also available, a combined static output feedback and static feed-forward controller is proposed. The synthesis problem is formulated as an $\mathscr{H}_\infty$-type design problem and can conveniently be solved by using linear matrix inequality (LMI) optimisations.

A great deal of research on developing lateral dynamics control systems employs a linear time-invariant (LTI) tyre model in which it is assumed that the tyre cornering stiffness is a constant parameter. However, the reliability of the LTI tyre model under different driving conditions, especially in evasive manoeuvers (e.g high lateral acceleration manoeuvers), has been a major concern and these models have limitations to represent nonlinear dynamics of the tyres. To deal with the problem of tyre nonlinearity, it is possible to synthesise the robust controller for the uncertain linear vehicle model with tyre cornering stiffness as an uncertain parameter within a known interval [9,16–18]. In order to have a more accurate tyre model and capture some important un-modelled tyre dynamics, the cornering stiffness can also be viewed as a time-varying uncertain parameter [19–21]. In this fashion, a linear

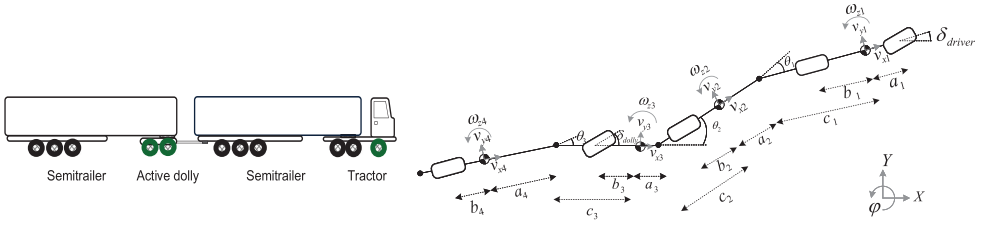

(a) Schematic of the A-double (b) Bicycle model of the A-double

Figure 1. A-double combination vehicle.

time-varying (LTV) tyre model can be used in which the cornering stiffness is treated as a time-varying uncertain parameter. In addition, the moments of inertia enter rationally in the system matrices of the linear vehicle model. Therefore, a descriptor-form system representation of the linear vehicle model is considered as a more convenient model to work with if compared to the standard state-space description, which would have rational dependence on the moments of inertia. The LMI optimisations are thus formulated based on a representation of the system in the descriptor form with affine parameter dependence in the system matrices. With affine parameter dependence in all the descriptor form matrices, one will then be faced LMI conditions with affine or polynomial parameter dependence, for which it is easier to obtain finitely many LMIs for synthesis (see [22]).

The paper is organised as follows. In the next section, a nonlinear and a linear dynamic model of the A-double combination vehicle (briefly denoted as the A-double) are described that are used for the analysis and synthesis purposes. The robust control synthesis is then introduced in Section 3. The application to the lateral control of the A-double is then explained in Section 4, where the simulation results are also presented. Finally, the paper is concluded with a summary and some concluding remarks in Section 5.

2. Vehicle models

In this study, two vehicle models for the A-double are considered: approximate (linear) and high-fidelity (nonlinear). First a detailed description of the linear vehicle model is provided which will be utilised in the design of the controller. This is then followed by brief explanation of a high-fidelity nonlinear vehicle model, referred to as the Volvo Transport Model (VTM), which is used in order to evaluate the designed controller.

2.1. Linear vehicle model in descriptor form

For mechanical systems, the descriptor form is usually obtained through the Lagrangian formulation, which is an alternative to the Newtonian approach. A major advantage of the Lagrangian formulation over Newtonian approach is that it can eliminate constraints and coupling forces between the units at the linking joints with a proper choice of the generalised coordinates [23]. Therefore in this study, a linear single-track model of the A-double is derived with five degrees of freedom (i.e. lateral and yaw motions of the tractor and three yaw motions of the towed units caused by the articulation joints) based on the Lagrangian formulation [24,25]. In the derivation of the proposed linear model, the longitudinal velocity v_x is considered as a constant value and all angles are assumed to be small.

Let us now briefly describe the Lagrangian approach with which a model is derived for the A-double. First the Lagrange function $L = T - V$ is introduced which is the difference between the total kinetic energy T and the total potential energy V of the system. Since the planar motion is considered in this model, the potential energy is set to zero. The Lagrangian equations are then obtained by differentiating the Lagrange function L with respect to the generalised coordinates and their time derivatives as follows:

$$\frac{\mathrm{d}}{\mathrm{d}t}\left(\frac{\partial L}{\partial \dot{q}_i}\right) - \frac{\partial L}{\partial q_i} = Q_i, \quad i = 1, \ldots, n. \tag{1}$$

In this equation, q_i is the i'th generalised coordinate, while Q_i represents the corresponding generalised external force. The vector of generalised coordinates is formed for the A-double as

$$q^T = [Y_1\ \varphi_1\ \theta_1\ \theta_2\ \theta_3], \tag{2}$$

where Y_1 and φ_1 are the lateral displacement of the centre of gravity and the yaw angle of the tractor, respectively. The remaining elements are the articulation angles between the attached units: θ_1 is the articulation angle between the tractor and the first semitrailer, θ_2 is the articulation angle between the first semitrailer and the dolly and θ_3 is the articulation angle between the dolly and the last semitrailer (see Figure 1(b)). The linear vehicle model is considered to be accurate under the assumption that steering and articulation angles are small. The schematic diagram of the linear vehicle model is depicted in Figure 1(b), where the axle groups in the driven axles of the tractor, the semitrailers and the dolly are lumped together into a single axle in the middle of each axle group.

The total kinetic energy of the system, which is the sum of the kinetic energies of the four units, is given as

$$T = \frac{1}{2}\sum_{j=1}^{4}(m_j v_j^2 + I_{z_j}\omega_{z_j}^2), \tag{3}$$

where v_j, ω_{z_j}, m_j and I_{z_j} are the translational velocity, the yaw rate, the mass and the yaw moment of inertia of the vehicle unit j, respectively. The generalised forces Q_i are also expressed as

$$Q_i = \sum_{k=1}^{N} F_k \frac{\partial r_k}{\partial q_i}, \tag{4}$$

where N is the number of forces and F_k's are the tyre forces with the position vector r_k and with the longitudinal and lateral components F_{x_k} and F_{y_k}, respectively. The longitudinal acceleration is considered to be zero which means that the vehicle is travelling with a constant longitudinal velocity. Therefore in the following, it is assumed that the longitudinal tyre forces are equal to zero.

Often in a linear bicycle model, a linear time-invariant (LTI) tyre model is used in which it is assumed that the tyre behaves linearly up to a certain slip angle. Hence, the lateral tyre force (F_{y_k}) on each axle is considered as a linear function of the lateral slip angle (α_{y_k}) as

$$F_{y_k} = C_{\alpha_k}\alpha_{y_k}, \quad k = 1_f, 1_r, 2, 3, 4, \tag{5}$$

where the proportionality constant C_{α_k} is the sum of the cornering stiffness of the tyres on each axle group and is determined by the slope of F_{y_k} versus α_{y_k} curve at $\alpha_{y_k} = 0$. In the bicycle vehicle model, it is assumed that the effects of all tyres on one axle are combined into one single virtual tyre. Also with the assumption that the axles in each axle group are combined together in the centre of the axle group, the subscripts 1_f, 1_r, 2, 3 and 4 denote the front axle of the tractor, the rear axles of the tractor, the first semitrailer axle group, the dolly axles and the second semitrailer axle group, respectively. In the linear models, it is usually assumed that the cornering stiffness remains constant irrespective of the slip angle. But in real-time, this assumption might not be valid, since the tyre cornering stiffness may

vary due to several factors like temperature, tyre normal load, road wear, tyre pressure, tyre-road friction and other unpredictable environmental factors that are difficult to measure directly. Therefore in more accurate models, the cornering stiffness needs to be viewed as a time-varying parameter.

In order to justify this, the system with the high-fidelity VTM model is simulated for a pseudo-random steering input as in Figure 2(b) at a longitudinal velocity of 80 km h^{-1}. In the VTM, the tyre forces are implemented by using the well-known Pacejka model [26], which captures many often-ignored tyre characteristics. The resulting variation of the lateral force versus the lateral tyre slip angle is presented in Figure 2(a). The proportionality constant, i.e. the ratio F_{y_k}/α_{y_k}, clearly changes when moving along this curve. In other words, Equation (5) would provide an accurate description of the tyre characteristics only with a C_{α_k} that varies with time. Moreover, the tyre dynamics are highly influenced by load variations, uneven road surfaces, tyre-road friction coefficient, temperature, inflation pressure and tyre conditions. This means that the curve in Figure 2(a) can cover even a larger area due to the changes caused by different factors. Therefore, in this study, a time-varying cornering stiffness parameter is considered by modifying Equation (5) as

$$F_{y_k} = C_{\alpha_k}(t)\alpha_{y_k}, \quad C_{\alpha_{k\min}} \leq C_{\alpha_k}(t) \leq C_{\alpha_{k\max}}, \tag{6}$$

where $C_{\alpha_{k\min}}$ and $C_{\alpha_{k\max}}$ are the lower and upper bounds of the cornering stiffness parameters of the kth axle group. These lower and upper bounds can be determined based on the typical variation range of the slip angle during the travel. Indeed the slopes of the lines that delimit the F_{y_k} versus α_{y_k} curves from above and below within the considered range of the slip angle could be used, respectively, as the upper and lower bounds for the cornering stiffness parameter (see Figure 2). With this assumption, it is possible to capture important un-modelled and nonlinear characteristics of the tyres to some extent by still working with a linear vehicle model.

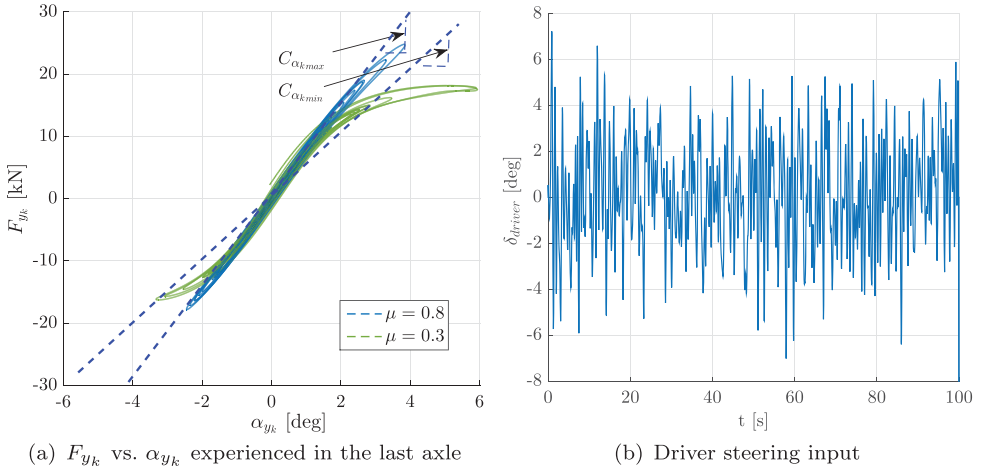

(a) F_{y_k} vs. α_{y_k} experienced in the last axle

(b) Driver steering input

Figure 2. Variation of F_{y_k} on the last axle of the second semitrailer as a function of α_{y_k} and corresponding applied random steering input for low ($\mu = 0.3$) and high ($\mu = 0.8$) tyre-road friction conditions (VTM simulation results) at longitudinal velocity of $v_x = 80$ km h^{-1}

As the last step of the derivation of a model based on Lagrangian formulation, one needs to insert the Equations (4) and (3) in (1) with positions, velocities and forces expressed in the global coordinate frame as can be found in Appendix 2. The final equation is then obtained in the following form

$$\mathcal{M}_q(\sigma(t))\ddot{q}(t) + \mathcal{C}_q(\sigma(t))\dot{q}(t) + \mathcal{K}_q(\sigma(t))q(t) = \mathcal{B}_q(\sigma(t))\delta_{dolly}(t) + \mathcal{H}_q(\sigma(t))\delta_{driver}(t). \tag{7}$$

The input signal $\delta_{dolly} \in \mathbb{R}^{n_u}$ is the control input vector and $\delta_{driver} \in \mathbb{R}^{n_d}$ is the driver steering input as the measurable disturbance input to the system, respectively. In our case, the considered control input δ_{dolly} is the steering angles applied to the dolly axles. The matrix $\mathcal{M}_q$ is the inertial matrix which is usually symmetric and positive definite, $\mathcal{C}_q$ is the damping matrix, $\mathcal{K}_q$ is the stiffness matrix, $\mathcal{B}_q$ is the force distribution matrix and $\mathcal{H}_q$ is the Jacobian of the constraint equation. The matrices $\mathcal{M}_q$, $\mathcal{C}_q$, $\mathcal{K}_q$, $\mathcal{B}_q$ and $\mathcal{H}_q$ based on the vehicle parameters are provided in Appendix 2. All vehicle parameters are assumed to be known except the moments of inertia of the two semitrailers and the cornering stiffness of the tyres in the axles of the vehicle.

A generic symbol $\sigma(t) \in \mathbb{R}^p$ is used to represent the vector of uncertain (possibly) time-varying parameters, whose rate-of-variation is denoted as $\nu(t) \triangleq \dot{\sigma}(t)$. As will be highlighted in the sequel, it is more convenient in our synthesis method to view σ_i as the percentage deviation of the i'th uncertain system parameter from its nominal value. It is assumed that lower and upper bounds are available for the uncertain parameter values as well as their derivatives. The uncertainty is thus described by introducing the sets

$$\begin{aligned} \mathbb{U} &\triangleq \{\sigma \in \mathbb{R}^p : \underline{\sigma}_i \le \sigma_i \le \bar{\sigma}_i,\ i = 1, \ldots, p\}, \\ \mathbb{V} &\triangleq \{\nu \in \mathbb{R}^p : \underline{\nu}_i \le \nu_i \le \bar{\nu}_i,\ i = 1, \ldots, p\}, \end{aligned} \tag{8}$$

where $\underline{*}_i/\bar{*}_i$ indicate the lower/upper bounds on $*_i$, respectively. A complete uncertain system description is obtained by accompanying (7) with $(\sigma(t), \nu(t)) \in \mathbb{U} \times \mathbb{V}, \forall t \ge 0$.

Now considering the state vector as $x_q^T \triangleq [q^T\ \dot{q}^T]$, the state-space model of the system of (7) in the descriptor form can be written as follows:

$$\underbrace{\begin{bmatrix} I & 0 \\ 0 & \mathcal{M}_q(\sigma(t)) \end{bmatrix}}_{\mathscr{E}(\sigma(t))} \underbrace{\begin{bmatrix} \dot{q}(t) \\ \ddot{q}(t) \end{bmatrix}}_{\dot{x}_q(t)} = \underbrace{\begin{bmatrix} 0 & I \\ -\mathcal{K}_q(\sigma(t)) & -\mathcal{C}_q(\sigma(t)) \end{bmatrix}}_{\mathscr{A}(\sigma(t))} \underbrace{\begin{bmatrix} q(t) \\ \dot{q}(t) \end{bmatrix}}_{x_q(t)} + \underbrace{\begin{bmatrix} 0 \\ \mathcal{B}_q(\sigma(t)) \end{bmatrix}}_{\mathscr{B}(\sigma(t))} \delta_{dolly}(t) + \underbrace{\begin{bmatrix} 0 \\ \mathcal{H}(\sigma(t)) \end{bmatrix}}_{\mathscr{H}_q(\sigma(t))} \delta_{driver}(t). \tag{9}$$

Two states Y_1 and φ_1 are removed from x_q to obtain the state-space model to be used in the design. It should be stressed that this is possible, thanks to the structure of the matrix $\mathcal{K}$. As a result, the state vector of the vehicle model $x_v \in \mathbb{R}^{n_v}$ is formed as

$$x_v = [\theta_1\ \theta_2\ \theta_3\ v_{y_1}\ \omega_{z_1}\ \dot{\theta}_1\ \dot{\theta}_2\ \dot{\theta}_3]^T, \tag{10}$$

where $\omega_{z_1} = \dot{\varphi}_1$. By removing the relevant row blocks from all matrices and also the relevant column blocks from $\mathscr{E}$ and $\mathscr{A}$, the dynamics of the system are expressed in the

descriptor framework as follows:

$$E_v(\sigma(t))\dot{x}_v(t) = A_v(\sigma(t))x_v(t) + H_v(\sigma(t))\delta_{driver}(t) + B_v(\sigma(t))\delta_{dolly}(t). \quad (11)$$

It should be noted that in the mechanical systems the descriptor matrix E_v is usually a non-singular matrix and is hence invertible. It is observed that the moments of inertia uncertainties appear naturally in the descriptor matrix E_v and the cornering stiffness of the tyres appear only in the matrices A_v, H_v and B_v.

2.2. Nonlinear vehicle model

The nonlinear high-fidelity vehicle model of the A-double, denoted as Volvo Transportation Model (VTM) is developed by Volvo Group Trucks Technology (VGTT). The VTM vehicle model is constucted by using a Matlab Simulink based toolbox developed for vehicle dynamics modelling and function development at VGTT. The VTM library contains detailed sub-models of the heavy vehicles such as chassis, frames, axles, tyres, suspensions, steering system, power-train and brakes. The Pacejka Magic Formula [26] is used to model the tyres and in this tyre model, a combined slip, dynamic relaxation, tyre normal load dependency and rolling resistance are used. Some vehicle combinations in the VTM library have been tested and validated against real test data and proved to be sufficiently accurate in predicting the actual vehicle behaviour [27,28].

3. Robust controller synthesis

The controller synthesis is formulated based on an $\mathscr{H}_\infty$-type design problem in which a bound has to be ensured on worst-case energy gains from finite-energy disturbance inputs to performance outputs of the system described in (11). In order to evaluate the performance of the system, a performance output signal $z \in \mathbb{R}^{n_z}$ is introduced as

$$z(t) = C_v x_v(t) + G_v \delta_{driver}(t) + D_v \delta_{dolly}(t), \quad (12)$$

where the matrices C_v, G_v and D_v will be determined depending on the considered z. These matrices might also have uncertain parameter dependence, which it is omitted here for simplicity. As a part of the general linear model, a measurement vector $y \in \mathbb{R}^{n_y}$ is also introduced. The signal y, which contains the available states of the system for feedback and also the driver steering input for feed-forward, is formed as

$$y(t) = S_v x_v(t) + R_v \delta_{driver}(t). \quad (13)$$

Since the $\mathscr{H}_\infty$ norm measures the input-to-output gain of the system for finite-energy input signals, one needs to restrict the class of disturbances under consideration in order to have a suitable problem formulation. This is especially the case here, since – with no measurement noise assumed – the driver steering angle δ_{driver} is the only external disturbance input applied to the system. In order to model the driver behaviour, a stable filter is introduced, which would typically be of low-pass or band-pass type. With this model, it is assumed that the frequency content of the driver steering is concentrated in a particular

range of frequency. A state-space realisation of the driver model can be represented as

$$\begin{aligned} \dot{x}_b(t) &= A_b x_b(t) + B_b w(t), \\ \delta_{driver}(t) &= C_b x_b(t) + D_b w(t), \end{aligned} \tag{14}$$

where $x_b \in \mathbb{R}^{n_b}$ and $w \in \mathbb{R}^{n_w}$ are the artificial state vector and disturbance input, respectively. Finally, the state-space realisation of the whole system is obtained by using the equations in (11)–(14) as follows:

$$\begin{aligned} \underbrace{\begin{bmatrix} E_v(\sigma(t)) & 0 \\ 0 & I \end{bmatrix}}_{E(\sigma(t))} \underbrace{\begin{bmatrix} \dot{x}_v(t) \\ \dot{x}_b(t) \end{bmatrix}}_{\dot{x}(t)} &= \underbrace{\begin{bmatrix} A_v(\sigma(t)) & H_v(\sigma(t))C_b \\ 0 & A_b \end{bmatrix}}_{A(\sigma(t))} x(t) + \underbrace{\begin{bmatrix} H_v(\sigma(t))D_b \\ B_b \end{bmatrix}}_{H(\sigma(t))} w(t) \\ &\quad + \underbrace{\begin{bmatrix} B_v(\sigma(t)) \\ 0 \end{bmatrix}}_{B(\sigma(t))} \delta_{dolly}(t), \\ z(t) &= \underbrace{\begin{bmatrix} C_v & G_v C_b \end{bmatrix}}_{C} x(t) + \underbrace{\begin{bmatrix} G_v D_b \end{bmatrix}}_{G} w(t) + \underbrace{\begin{bmatrix} D_v \end{bmatrix}}_{D} \delta_{dolly}(t), \\ y(t) &= \underbrace{\begin{bmatrix} S_v & R_v C_b \end{bmatrix}}_{S} x(t) + \underbrace{\begin{bmatrix} R_v D_b \end{bmatrix}}_{R} w(t). \end{aligned} \tag{15}$$

In this representation, $x \in \mathbb{R}^{n_x}$ is the extended state vector and the dimensions of the system matrices can be identified from compatibility. The system representation described so far is assumed to be obtained in a way that is suitable for synthesis (e.g. no unstable states that are not controllable). Nevertheless, since a robust static output feedback synthesis problem is considered for an uncertain system, it is left to the synthesis LMIs to implicitly specify the necessary requirements on the system.

The controller synthesis is considered based on static output feedback in a way that implicitly includes static feed-forward thanks to the construction of the measurement signals as in (13). In order to formulate a static output feedback synthesis problem, it is only required to express the control input δ_{dolly} as

$$\delta_{dolly}(t) = Ky(t), \tag{16}$$

where K is the gain matrix to be designed and contains two components (i.e. $K = [K_{fb}\, K_{ff}]$): the feedback gain K_{fb} and the feed-forward gain K_{ff}. This approach is thus a one-degree of freedom controller synthesis formulated as a standard static output feedback. Note that in order to have a two-degrees of freedom synthesis, the feed-forward filter needs to be dealt with separately.

The $\mathscr{H}_\infty$ synthesis aims at ensuring bounds on the energy gain from the disturbance input w to the performance output z. An $\mathscr{H}_\infty$ synthesis problem can then be formulated as follows: given a linear model described as in (15), synthesise a gain matrix K such that the controlled closed-loop system is stable and the following $\mathscr{L}_2$-gain condition is satisfied:

$$\|z\|_2 < \gamma \|w\|_2, \forall w(\cdot) \text{ with } 0 < \|w\|_2 < \infty \text{ and } x(0) = 0. \tag{17}$$

In this expression, the scalar γ is the desired level of $\mathcal{L}_2$-gain performance. When the system and the controller are linear time-invariant, the performance objective given in (17)

is an $\mathscr{H}_\infty$ constraint on the transfer function/matrix from w to z and can be re-expressed equivalently as

$$\|\mathcal{T}_{zw}\|_\infty \triangleq \sup_{Re\{s\}>0} \|\mathcal{T}_{zw}(s)\| < \gamma, \tag{18}$$

where $\|\cdot\|$ represents the maximum singular value.

Now a procedure for $\mathscr{H}_\infty$ static output feedback synthesis is described. The synthesis is based on extended (dilated) LMI conditions adapted from [29] with a modification to be applicable to the descriptor systems as provided from the previous work in [30]. The basic idea behind the dilation is that the state-feedback gain K is constructed independently of the Lyapunov matrix Y in order to reduce the potential conservatism [29]. In this fashion, the controller is constructed with the gain matrix obtained according to

$$K = NW^{-1}, \tag{19}$$

where $N \in \mathbb{R}^{n_u \times n_y}$ and $W \in \mathbb{R}^{n_y \times n_y}$ are the matrix variables to be determined. The matrix inequality for static output feedback synthesis is now recalled from [29] and expressed for the standard state-space description of (15). In this fashion, the LMI condition is obtained as

$$\mathsf{He}\begin{bmatrix} -\phi W & \phi(SY - WS) & \phi R & 0 \\ E^{-1}BN & (E^{-1}AY + E^{-1}BNS) & E^{-1}H & 0 \\ 0 & 0 & -\frac{\gamma}{2}I & 0 \\ DN & (CY + DNS) & G & -\frac{\gamma}{2}I \end{bmatrix} \prec 0, \tag{20}$$

where $\mathsf{He}\,\mathcal{M} \triangleq \mathcal{M} + \mathcal{M}^T$ and $\phi \in \mathbb{R}^+$ is an arbitrary (yet fixed) scalar. In order to derive an LMI condition that is applicable for descriptor systems, one needs to apply a congruence transformation to (20) with the block-diagonal matrix $\mathsf{blockdiag}(I, E, I, I)$.

In conclusion, the $\mathcal{L}_2$-gain constraint of (17) will be satisfied if there exist $0 \prec Y = Y^T \in \mathbb{R}^{n_x \times n_x}$, N and W such that the following LMI condition is satisfied:

$$\mathcal{N} \triangleq \mathsf{He}\begin{bmatrix} -\phi W & \phi(SY - WS)E^T & \phi R & 0 \\ BN & (AY + BNS)E^T & H & 0 \\ 0 & 0 & -\frac{\gamma}{2}I & 0 \\ DN & (CY + DNS)E^T & G & -\frac{\gamma}{2}I \end{bmatrix} \prec 0. \tag{21}$$

Note that this is an LMI condition when ϕ is fixed. Hence, in order to find the smallest value of γ, one can perform minimisations over γ for a grid of ϕ values. The gain matrix is then computed as in (19) with the N and Y matrices associated with the smallest γ.

By then calculating K from (19) and inserting (16) in the first two equations of (15), a new state-space realisation of the closed-loop system is obtained as

$$\begin{aligned} E\dot{x}(t) &= \underbrace{(A + BKS)}_{\mathcal{A}} x(t) + \underbrace{(H + BKR)}_{\mathcal{H}} w(t), \\ z(t) &= \underbrace{(C + DKS)}_{\mathcal{C}} x(t) + \underbrace{(G + DKR)}_{\mathcal{G}} w(t). \end{aligned} \tag{22}$$

In the sequel, it will be discussed how the LMI condition in (21) can be used to synthesise a robust controller for the system (15) whose dynamics depend on (time-invariant or/and time-varying) uncertain parameters. The system matrices of the plant given in (15) have affine parameter dependence (i.e. $E(\sigma) = E_0 + \sum_{i=1}^{p} E_i\sigma_i$, where $E_0, E_1, \ldots, E_p$ are known fixed matrices). Thanks to this affine dependency, the optimisation problem can be formulated in a way to ensure stability as well as the performance objective of (17) for all parameter values $\sigma \in \mathbb{U}$. In this fashion, the solvability condition (21) appears as a parameter-dependent LMI (PLMI) that needs to be satisfied over the whole uncertainty region, that is, in the form

$$\mathcal{N}(\sigma) = \mathcal{N}_0 + \mathcal{N}_1\sigma_1 + \cdots + \mathcal{N}_p\sigma_p \prec 0, \quad \forall\sigma \in \mathbb{U}. \tag{23}$$

In order to have a less conservative design of the controller, the Lyapunov matrix Y can be chosen to depend on the uncertain parameters (i.e. $Y = Y_0 + \sum_{i=1}^{p} Y_i\sigma_i$). In the case of uncertain time-varying parameter σ_i, a modification in the (2,2) block of $\mathcal{N}$ in (20) is needed by adding $-\sum_{i=1}^{p}(\partial Y_i/\partial\sigma_i)\nu_i$ and consequently adding $-E\sum_{i=1}^{p}(\partial Y(\sigma)/\partial\sigma_i)\nu_i E^T$ in the (2,2) block of $\mathcal{N}$ in (21) as follows:

$$\mathcal{N}(\sigma,\nu) \triangleq \mathsf{He}\begin{bmatrix} -\phi W & \phi(SY - WS)E^T & \phi R & 0 \\ BN & \left(AY + BNS - \frac{1}{2}E\sum_{i=1}^{p}\frac{\partial Y}{\partial\sigma_i}\nu_i\right)E^T & H & 0 \\ 0 & 0 & -\frac{\gamma}{2}I & 0 \\ DN & (CY + DNS)E^T & G & -\frac{\gamma}{2}I \end{bmatrix} \prec 0,$$
$$\forall(\sigma,\nu) \in \mathbb{U}\times\mathbb{V}. \tag{24}$$

It should be noted that the matrices W and N are chosen without any dependence on the unmeasurable parameters and the other matrices are assumed as affine-parameter-dependent matrices. In (24), the parameter dependence is suppressed in the system matrices and Y for notational simplicity. In this setting, the LMI conditions need to be satisfied over the whole region of uncertainty, i.e. at infinitely many points.

In order to formulate optimisation problems based on finitely many LMIs, a relaxation scheme or a gridding technique can be applied. The gridding methods might result in better performance than relaxation schemes but the computational burden is much higher [31]. Moreover, if the gridding is not fine enough, one might obtain a controller which in fact violates the performance requirement. Therefore, a relaxation scheme is employed that is suitable for the considered uncertainty region (see [32] and the references therein). Since the parameter-dependence is affine and the uncertainty region is a hyper-rectangle, the multi-convexity approach of [33] can be adopted. In this case, the LMI conditions are imposed only at the vertices of the parameter boxes in (8):

$$\mathcal{N}(\sigma,\nu) \prec 0, \quad \forall(\sigma,\nu) \in \mathbb{U}_{vex}\times\mathbb{V}_{vex}. \tag{25}$$

In this condition, $\mathbb{U}_{vex}$ and $\mathbb{V}_{vex}$ are the sets of 2^p vertices of each parameter box in (8) and are identified as

$$\mathbb{U}_{vex} \triangleq \{\sigma \in \mathbb{R}^p : \sigma_i \in \{\underline{\sigma}_i, \bar{\sigma}_i\},\ i = 1,\ldots,p\},$$
$$\mathbb{V}_{vex} \triangleq \{\nu \in \mathbb{R}^p : \nu_i \in \{\underline{\nu}_i, \bar{\nu}_i\},\ i = 1,\ldots,p\}. \tag{26}$$

In this fashion by employing the above relaxation scheme, considering p uncertain parameters, infinitely many LMIs will be decreased to 2^{2p} LMIs. In order to ensure that (25) is sufficient for (24), one needs to impose an additional constraint. This constraint is defined based on the concept of multi-convexity, that is, convexity with respect to each uncertain parameter while others are assumed to be constant [33]. To this end, in addition to imposing the LMI constraints (25) on the vertices of $\mathbb{U}_{vex} \times \mathbb{V}_{vex}$, the second derivatives of the LMI constraint with respect to each uncertain parameter should also be positive semi-definite:

$$\mathcal{P}_j(\sigma, \nu) = \frac{\partial^2 \mathcal{N}(\sigma, \nu)}{\partial \sigma_j^2} \succeq 0, \quad \forall (\sigma, \nu) \in \mathbb{U}_{vex} \times \mathbb{V}_{vex}, \ \ j = 1, \ldots, p. \tag{27}$$

Note that (27) is to be satisfied only at the vertices of the hyper-rectangle thanks to the fact that the inequality has affine dependence on the uncertain parameters. For the systems with the parameter dependency as in (15), the multi-convexity conditions imposed at the vertices of the hyper-rectangle read as

$$\mathcal{P}_j(\sigma, \nu) = \mathsf{He} \begin{bmatrix} 0 & 2\phi S Y_j E_j^T & 0 & 0 \\ 0 & \begin{array}{c} 2(AY_jE_j^T + A_jY_jE^T + A_jYE_j^T \\ +B_jNSE_j^T) - E_j \sum_{i=1}^{p} \dfrac{\partial Y}{\partial \sigma_i} \nu_i E_j^T \end{array} & 0 & 0 \\ 0 & 0 & 0 & 0 \\ 0 & 2CY_jE_j^T & 0 & 0 \end{bmatrix} \succeq 0. \tag{28}$$

Since this is a non-strict LMI, which implicitly contains an equality condition, it needs further attention for a successful application of the synthesis method. For a numerically reliable implementation, one needs to slightly modify (25) in such a way that the resulting multi-convexity constraint turns (28) into a strictly feasible LMI. Conditions modified in this fashion are expressed as follows:

$$\begin{aligned} \mathcal{T}_1(\sigma) \left(\mathcal{N}(\sigma, \nu) + \sum_{j=1}^{p} \sigma_j^2 M_j \right) \mathcal{T}_1^T(\sigma) &\prec 0, \quad \forall (\sigma, \nu) \in \mathbb{U}_{vex} \times \mathbb{V}_{vex}, \\ \mathcal{T}_2(\sigma) \left(\mathcal{P}_j(\sigma, \nu) + 2M_j \right) \mathcal{T}_2^T(\sigma) &\succcurlyeq 0, \quad \forall (\sigma, \nu) \in \mathbb{U}_{vex} \times \mathbb{V}_{vex}, \ \ j = 1, \ldots, p, \\ M_j &\succcurlyeq 0, \quad j = 1, \ldots, p. \end{aligned} \tag{29}$$

Note that M_j's are introduced in these inequalities as slack variables in accordance with the suggestion of [33] and they can be specialised to $M_j = \epsilon_j I$ with scalar $\epsilon_j \geq 0$ to reduce the number of variables if necessary. With this modification, it is more convenient to choose σ_j's as the deviations of the uncertain system parameters from their nominal values. Indeed it then becomes possible to recover the standard nominal synthesis LMI when there is no uncertainty (i.e. $\sigma_j \to 0$), since the multi-convexity conditions would then always be satisfied with sufficiently large ϵ_j's. For possible further conditioning, the congruence transformations with invertible $\mathcal{T}_1$ and $\mathcal{T}_2$ is also introduced based on our experience.

For instance, if the standard system representation is well-conditioned, one might prefer to use its realisation matrices $(E^{-1}A, E^{-1}B, \ldots)$ in the LMI conditions instead of using (25). To this end, one would simply choose $\mathcal{T}_1 = \mathsf{blockdiag}(I, E^{-1}, I, I)$. Finally, it should be noted that the positive-definiteness condition $Y_0 + \sum_{i=1}^{p} Y_i \sigma_i \succ 0$ should also be imposed at the vertices of the hyper-rectangle.

4. Controller design and simulations

In this section, the synthesis procedures developed in the previous sections are applied to the linear vehicle model of the A-double. The associated simulation results are then provided by using the nonlinear VTM vehicle model. It is assumed that both dolly axles are steered with the same amount of the steering angle. The LMI optimisation problems in this paper are solved in Matlab by using YALMIP [34] as the interface and SeDuMi [35] as the SDP solver.

4.1. Control design using linear vehicle model

The main objective of the control system is to enhance the lateral performance of the A-double by attenuating undesired dynamic responses in the towed units especially during high-speed critical driving situations such as obstacle-avoidance. The A-double is considered with a total weight of about 80 tonnes and a total length of 31.5 m. In order to achieve the lateral performance improvement, the yaw motion oscillations in the last semitrailer are mitigated via active steering of the dolly axles. In order to minimise the yaw rate of the last semitrailer without leading to undesirable behaviour in the dolly, the performance signal is chosen as $z = \left[\omega_{z_4}\ \delta_{dolly}\right]^T$, where ω_{z_4} is the yaw rate of the last semitrailer and δ_{dolly} is the steering control input applied to the dolly axles.

All vehicle parameters are assumed to be known except the moments of inertia of the first and second semitrailers (I_{z_2} and I_{z_4}), and the cornering stiffness of the tyres in the axles of the vehicle ($C_i, i = 1_f, 1_r, 2, 3, 4$). C_{1_f} is the sum of the tyre cornering stiffness on the first axle of the tractor. The sum of the tyre cornering stiffness of the second and third axles of the tractor is equal to C_{1_r}. In the same way, the total sum of the tyre cornering stiffness of joint axles of the first semitrailer, the dolly and the second semitrailer are defined as C_2, C_3, C_4, respectively. The model thus has seven uncertain parameters, which are listed in Table 1 together with their minimum and maximum values. It is assumed that for each tyre, the cornering stiffness varies inside a sector delimited by two lines passing through the origin in Figure 2: a line with the minimum slope as $C_{\alpha_{k\min}}$ and another line with the maximum slope as $C_{\alpha_{k\max}}$ covering the area of interest in the time-varying F_{y_k} versus α_{y_k} curve. It should be noted that I_{z_2} and I_{z_4} are time-invariant parameters, while all of the C_i's are treated as time-varying parameters. The rates of variation of time-varying uncertain parameters are bounded by $|\dot{C}_i| \leq 50, i = 1_f, 1_r, 2, 3, 4$, which is observed to be a suitable choice for the considered scenarios depicted in Figure 2.

It is also noted from Table 1 that the uncertain parameters used in our system representation are defined as percentage deviations from the nominal values, e.g. $\sigma_1 = I^{\circ}_{z_2}(1 + \sigma_1)$, where $I^{\circ}_{z_2} = (I^{\min}_{z_2} + I^{\max}_{z_2})/2$ is viewed as the nominal value. In the uncertain system of (15), the system matrices depend affinely on σ_i and the particular form of the

Table 1. Minimum and maximum values of uncertain parameters.

Parameter	Description	Min	Max	Unit
$I_{z_2} = I^{\circ}_{z_2}(1+\sigma_1)$	Yaw moment of inertia of 1st semitrailer	$2.5 \cdot 10^5$	$4.5 \cdot 10^5$	kg m^2
$I_{z_4} = I^{\circ}_{z_4}(1+\sigma_2)$	Yaw moment of inertia of 2nd semitrailer	$2.5 \cdot 10^5$	$4.5 \cdot 10^5$	kg m^2
$C_{1_f} = C^{\circ}_{1_f}(1+\sigma_3)$	Cornering stiffness of truck front axle	$3 \cdot 10^5$	$5 \cdot 10^5$	N rad^{-1}
$C_{1_r} = C^{\circ}_{1_r}(1+\sigma_4)$	Cornering stiffness of truck driven axles	$9 \cdot 10^5$	$12 \cdot 10^5$	N rad^{-1}
$C_2 = C^{\circ}_2(1+\sigma_5)$	Cornering stiffness of 1st semitrailer axles	$9.5 \cdot 10^5$	$14 \cdot 10^5$	N rad^{-1}
$C_3 = C^{\circ}_3(1+\sigma_6)$	Cornering stiffness of dolly axles	$9 \cdot 10^5$	$13 \cdot 10^5$	N rad^{-1}
$C_4 = C^{\circ}_4(1+\sigma_7)$	Cornering stiffness of 2nd semitrailer axles	$9.5 \cdot 10^5$	$14 \cdot 10^5$	N rad^{-1}

$C_{1_f} = C_{\alpha_1}$, $C_{1_r} = C_{\alpha_2} + C_{\alpha_3}$, $C_2 = C_{\alpha_4} + C_{\alpha_5} + C_{\alpha_6}$, $C_3 = C_{\alpha_7} + C_{\alpha_8}$, $C_4 = C_{\alpha_9} + C_{\alpha_{10}} + C_{\alpha_{11}}$

dependency is identified as

$$E = E_0 + \sum_{j=1}^{2} E_j\sigma_j, \quad A = A_0 + \sum_{j=3}^{7} A_j\sigma_j, \quad B = B_0 + B_6\sigma_6, \quad H = H_0 + H_3\sigma_3,$$

where E_j, A_j, B_j and H_j are known fixed matrices which can be obtained by using the equations and expressions given in Section 2.1 and in Appendix 2. The E matrix has dependence on the moments of inertia, while the A matrix depends on the cornering stiffness of the tyres. In fact the reason behind using the descriptor form of the state space model is to avoid dealing with rational dependence on the moments of inertia in the standard state-space form. Thus the approach of [22] is followed to formulate tractable LMI problems for controller synthesis. To reduce conservatism a parameter-dependent Lyapunov matrix is assumed of the form

$$Y(\sigma) = Y_0 + Y_1\sigma_1 + Y_2\sigma_2 + Y_3\sigma_3 + \cdots + Y_7\sigma_7.$$

In this study, only one (out of 8) state (θ_2) and one external signal (δ_{driver}) are considered as available measurements: $y = [\theta_2\ \delta_{driver}]^T$. Thus, a combined version of static output feedback and feed-forward controllers is synthesised in the presence of parameter uncertainties. It is assumed that the frequency content of the driver steering is concentrated within the frequency range $[f_l, f_h] = [0.05, 3.5]$ Hz. Note that in a single lane change, a human driver is capable of a steering frequency of maximum 3.5 Hz, as stated in [36]. The driver is hence modelled with a second-order band-pass filter with a pass-band of [0.05, 3.5] Hz.

The controller gain is synthesised by minimising the value of γ under (29) and $Y(\sigma) \succ 0, \forall\sigma \in \mathbb{U}_{vex}$. The matrices M_j are chosen as $M_j = \epsilon_j I$ and good numerical conditioning is obtained with $\mathcal{T}_1 = \mathsf{blockdiag}(I, E^{-1}, I, I)$ and $\mathcal{T}_2 = \mathsf{blockdiag}(I, 10^{-6}I, I, I)$. The enormous computational complexity of the problem (32903 constraints in terms of 17 variables) prevented an extensive search over ϕ. After some simplified design exercises, the range is first reduced to [3, 10] and a line search is performed with 14 grid points. The minimum γ values and the associated controllers are found with parameter-dependent and parameter-independent Y as follows:

$$Y = Y_0 + \Sigma_{j=1}^{p} Y_j\sigma_j : \phi = 5.0, \quad \gamma = 5.0, \quad K = [-0.5165 \ -0.0274],$$
$$Y = Y_0 \qquad\qquad : \phi = 5.5, \quad \gamma = 9.5, \quad K = [-0.4401 \ -0.0612].$$

It is observed from the γ values that the choice of parameter-dependent Y leads to significantly improved performance. In the sequel, the system with the controller corresponding to the parameter-dependent Lyapunov function is analysed.

4.2. Verification of controller effectiveness and robustness

Certification of a controller is admittedly a challenging task for uncertain systems and more so when the uncertain parameters are time-varying. In order to verify the effectiveness and robustness of our controller, the following steps are performed both for the controlled and uncontrolled cases:

- Frozen parameter analysis with the linear model to illustrate the effectiveness and robustness of the controller in the case of time-invariant parameters and to determine the worst-case parameter values
- Frequency domain analysis based on the data obtained from VTM simulations (with worst-case parameter values) in which a steering input with rich frequency content is applied
- Time domain analysis based on the data obtained from VTM simulations (with worst-case parameter values) in which single sine wave steering inputs are applied with varying frequencies
- Analysis of time histories of various physical signals in the case of a single sine wave steering input with worst-case frequency

These steps are explained in detail in the following subsections.

4.2.1. Frozen Parameter Analysis

In order to evaluate the synthesised controller, first the magnitude plot of the transfer function $\mathcal{T}_{\omega_{z_4}\omega_{z_1}}$ from ω_{z_1} to ω_{z_4} is analysed. The magnitudes of this transfer function can be viewed as a lateral performance measure known as rearward amplification (RA) in the second semitrailer in the frequency domain. The rearward amplification is defined as the ratio between the lateral acceleration or yaw rate of the towed units to that of the first unit. Smaller values of RA imply lower oscillations in the towed units and consequently indicate better lateral dynamic performance. The RA in the frequency domain, denoted as RA^f, is then defined as the peak magnitude of the transfer function $\mathcal{T}_{\omega_{z_i}\omega_{z_1}}$ from ω_{z_1} to ω_{z_i} and is thus obtained as

$$\mathrm{RA}_i^f \triangleq \max_{\omega} |\mathcal{T}_{\omega_{z_i}\omega_{z_1}}(j\omega)| = \max \left| \frac{\mathcal{T}_{\omega_{z_i} w}(j\omega)}{\mathcal{T}_{\omega_{z_1} w}(j\omega)} \right|, \quad i = 2, 3, 4, \tag{30}$$

where ω_{z_1} and ω_{z_i} are the yaw rates of the tractor and the vehicle unit i in the A-double, and $\mathcal{T}_{\omega_{z_1} w}$ and $\mathcal{T}_{\omega_{z_i} w}$ are the transfer functions from w to ω_{z_1} and ω_{z_i}, respectively.

In order to evaluate the performance of the LTI vehicle model, a frozen parameter analysis is performed. In this approach, the parameter values are assumed to be fixed and the resulting transfer functions are analysed. Since all cornering stiffness parameters are time-varying uncertainties with trajectories varying within magnitude and derivative bounds, good performance should be achieved also when the derivative is zero. It should be noted

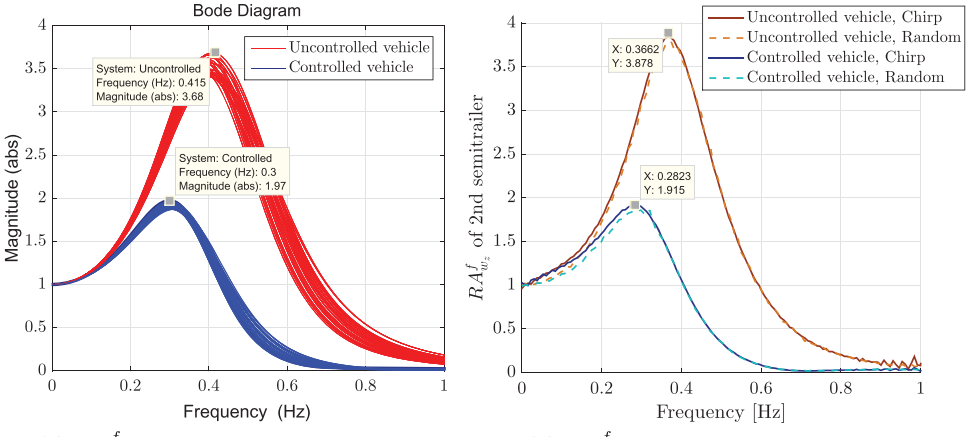

(a) $RA^f_{\omega_{z4}}$ in the linear vehicle model (b) $RA^f_{\omega_{z4}}$ in the VTM vehicle model

Figure 3. Yaw rate RA^f_4 versus frequency plots obtained from the linear model by using magnitude plots and in the VTM model by using chirp-steering (solid curves) and random-steering methods (dashed curves) at $v_x = 80\,\text{km h}^{-1}$.

that the zero derivative should be within the minimum and maximum derivative values, which is the case in our design.

Figure 3(a) presents the overlay plots for different values of the uncertain parameters within the uncertainty region (100 top worst cases chosen among $4^7 = 16,384$ uniformly-spaced grid points) for both the uncontrolled and the controlled system. It is observed from this figure that the imposed $\mathscr{L}_2$-gain constraint pushes down significantly the peak magnitudes in the transfer function for different perturbed parameters values. The robustness of the controller can be inferred from the observation that the curves for the controlled vehicle cover a relatively smaller area in comparison with the curves for the uncontrolled vehicle.

In order to perform selective simulations in the sequel that verify robustness in the face of nonlinearities and time-variations, the worst cases are identified from Figure 3 together with the associated parameter values. The worst-case $\mathscr{H}_\infty$ norms (i.e. peak magnitude over frequency) for the uncontrolled and controlled cases are determined as 3.68 (at the frequency of 0.42 Hz) and 1.97 (at the frequency of 0.3 Hz), respectively. The parameter values associated with both worst-cases are determined as the following:

$$I_{z2} = 4.5 \cdot 10^5 \text{ and } I_{z4} = 4.5 \cdot 10^5 \text{ [in kg m}^2\text{]},$$
$$C_{1_f} = 3 \cdot 10^5, C_{1_r} = 12 \cdot 10^5, C_2 = 9.5 \cdot 10^5, C_3 = 9 \cdot 10^5 \text{ and } C_4 = 9.5 \cdot 10^5 \text{[in N rad}^{-1}\text{]}.$$

4.2.2. Frequency domain analysis based on VTM simulations

In order to further analyse and verify the performance of the controller, simulations are performed with the high-fidelity VTM model by fixing the parameters to the worst-case values obtained from frozen parameter analysis. For the cornering stiffness parameters, this is done by adjusting the slope of the F_{y_k} versus α_{y_k} curve in the linear region. Excitation of nonlinear behaviour would hence correspond to variations of the uncertain parameters

in time in our uncertain system model. Two frequency-domain excitation approaches are then used in order to validate the effectiveness of the controller in the high-fidelity VTM model.

In the first approach, the simulations are performed by using a chirp (swept-sine) as the driver steering input with an amplitude of 0.86° and with a frequency sweep from 0 to 1 Hz in 180 s [37]. In the second approach, a random driver steering input is chosen in which both the frequency and amplitude of the steering input are varied randomly and continuously. In order to ensure that enough data is collected to capture the whole frequency range, the steering input is applied for at least 12 min as recommended in ISO 14791 [38,39]. The applied chirp and random steering inputs are shown in Figure 4. It should be noted that in the case of uncontrolled vehicle, the steering input applied to the dolly axles is zero. These admittedly unrealistic steering inputs are chosen since we still aim for a frequency-domain analysis of the rearward amplification based on Fast Fourier Transforms (FFTs). In this analysis, the RA^f values are obtained at a grid of frequencies by first dividing the FFT of the yaw rate in the second semitrailer with the FFT of the yaw rate in the tractor and then computing the magnitude.

Figure 3(b) presents the empirical yaw rate RA^f estimates when the parameters are set to their worst-case values. The maximum RA^f over the considered frequency range for the uncontrolled and controlled cases are determined as 3.88 (at the frequency of 0.37 Hz) and 1.91 (at the frequency of 0.28 Hz), respectively. The general shapes of the curves resemble the linear analysis results seen in Figure 3(a). However the maximum RA^f value in the VTM model in the uncontrolled case is a bit higher and in the controlled case slightly smaller than the linear model. It is also interesting to see a great agreement between the results obtained from the random and chirp steering input approaches.

In order to facilitate a better evaluation of the overall vehicle behaviour, the yaw rate and lateral acceleration RA^f of the towed vehicle units are all presented in Figure 5. We first note from Figure 5(b) that the RA values for the lateral acceleration in the semi-trailer are also reduced significantly by favour of control. To ensure desirable vehicle behaviour, we need to check whether there is any undesirable increase in the RA values of the other

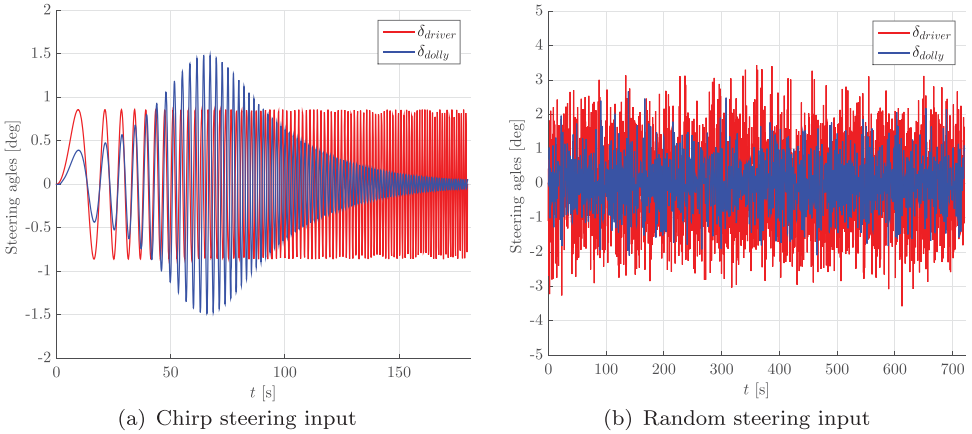

(a) Chirp steering input (b) Random steering input

Figure 4. Applied driver steering input (for both controlled and uncontrolled vehicle) and dolly steering input (for controlled vehicle) in the VTM vehicle model at $v_x = 80$ km h^{-1}.

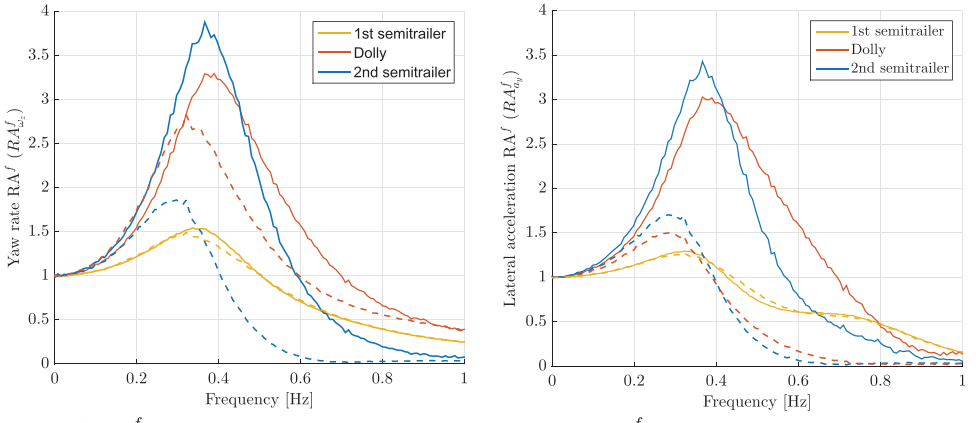

(a) $RA^f_{\omega_z}$ in the VTM vehicle model (b) $RA^f_{a_y}$ in the VTM vehicle model

Figure 5. Yaw rate and lateral acceleration RA^f for the towed vehicle units versus frequency plots in the VTM model by using random-steering input at $v_x = 80$ km h^{-1}; uncontrolled vehicle (solid curves) and controlled vehicle (dashed curves)

units in the controlled case in reference to the passive case. For the first semi-trailer, we detect from Figure 5(b) a harmless increase in the RA values of the lateral acceleration within the frequency band $[0.4, 0.6]$ Hz. We notice from Figure 5(a) a more noteworthy increase in the RA values of the yaw rate in the dolly below 0.3 Hz. Since the RA increases in both of these cases would hardly jeopardise the stability, the controlled vehicle can be considered to have superior overall performance.

4.2.3. Time domain analysis for single lane change simulations

In this subsection, the performance of the controller is analysed in realistic single lane change (SLC) manoeuvers, which are modelled by single sine-wave driver steering inputs (see Figure 7). The simulations are performed with uncertain parameters set to their worst-case values and with SLC manoeuvers applied with selected frequencies within a range. The analysis is then performed based on the time-domain computation of rearward amplification.

The yaw rate RA^t of the vehicle unit i in the A-double is defined based on the time-domain signals as

$$\mathrm{RA}^t_i \triangleq \frac{\|\omega_{z_i}\|_\infty}{\|\omega_{z_1}\|_\infty}, \quad i = 2, 3, 4, \tag{31}$$

where $\|\cdot\|_\infty$ represents the peak value over time. It is important to note at this point that the RA varies with varying steering input frequency in both frequency and time domain computations, which are likely to differ from each other. In fact, the time-domain values are obtained as a result of the transient behaviour of the vehicle, while the frequency domain RA^f values are mainly obtained based on the steady-state response. Though highly correlated, the two definitions lack a clear mathematical relation with each other. Furthermore, it is hard to compute RA^t analytically for linear systems, while the RA^f can be calculated directly from the realisation matrices and covers the entire frequency range [13,40].

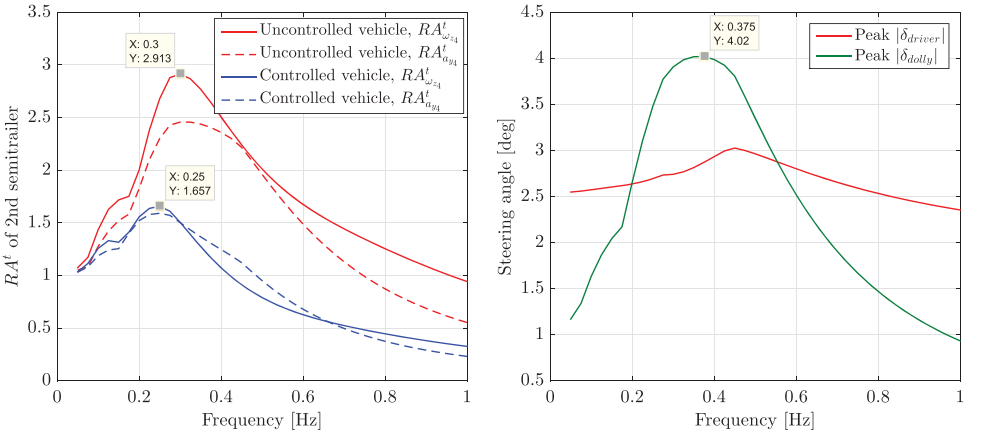

(a) $RA^t_{\omega_{z_4}}$ in the VTM vehicle model (b) Peak values of the driver and dolly steering inputs

Figure 6. Yaw rate RA^t_4 versus frequency and peak values of the applied driver steering input (in both the uncontrolled and controlled cases) and the dolly steering input (in the controlled case).

The SLC manoeuvers are simulated at a fixed longitudinal velocity of 80 km h^{-1} with steering input frequencies ranging from 0.05 to 1 Hz. To facilitate a fair comparative evaluation, the amplitude of the driver steering input is adjusted in each case in a way to have a peak lateral acceleration of 1.5 m s^{-2} at the first axle of the tractor unit (i.e. peak $|a_{y_{11}}| = 1.5\,\mathrm{m\,s^{-2}}$). This is done mainly to ensure that the tyre forces remain mostly in the linear region of the tyre force curve. However, this level of lateral acceleration was also considered as a reasonable value for investigating heavy vehicles with a lateral acceleration RA^t of 2 or higher. For instance for a heavy vehicle with a lateral acceleration RA^t of 2 and a peak of $|a_{y_{11}}| = 1.5\,\mathrm{m\,s^{-2}}$, the peak lateral acceleration of the last unit will be 3 m s^{-2}, which is less than the rollover threshold level of 3.5 m s^{-2} recommended according to Australian Performance Based Standard [41].

The variation of (both yaw rate and lateral acceleration) RA^t_4 versus the steering input frequency is presented in Figure 6(a) for the vehicle with the parameter values associated with the worst-case performance. This is accompanied by Figure 6(b) in which the peak values of the applied driver and dolly steering angles that lead to a peak value of $|a_{y_{11}}| = 1.5\,\mathrm{m\,s^{-2}}$ are displayed. Figure 6(a) clearly illustrates the effectiveness of the controller in reference to the passive case. The robust performance of the controller is also verified by this plot in that the RA^t stays below 2 even in the worst case. As identified from Figure 6(b), the reductions in the RA^t values in the controlled case are achieved by applying dolly steering angles with peak values below 4.02°. It should finally be noted that the RA^t values in Figure 6(a) are smaller than the RA^f values in Figure 3(b), but both RAs still show similar variation with frequency.

4.2.4. Analysis of a single lane change manoeuver with worst-case frequency

The analysis results from the previous subsection can be used to detect the worst-case steering input frequencies, for which the RA^t values become largest. From Figure 6(a), the worst-case SLC frequencies in the uncontrolled and controlled cases are identified as 0.3 and 0.25 Hz, respectively. In the sequel, the time histories of various physical signals

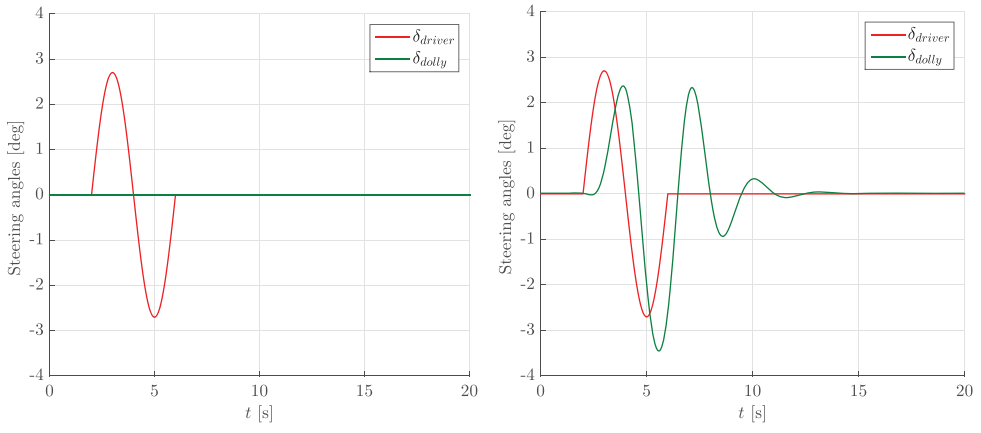

(a) Uncontrolled vehicle (b) Controlled vehicle

Figure 7. Applied steering angles in the first axle of the tractor and the axles of the dolly in a SLC (v_x = 80 *km* h^{-1}, driver steering frequency = 0.25 Hz, peak $|a_{y_{11}}|$ = 1.5 m s^{-2}).

associated with different units are analysed closely, both in uncontrolled and controlled cases, when the steering input frequency is set to 0.25 Hz. Although the benefit of control is observed more strikingly at 0.3 Hz, we have chosen the worst-case frequency associated with the controlled case especially to illustrate the robustness of the controller.

The driver steering input applied in this case and the resulting dolly steering angles are displayed in Figure 7. The yaw rate variation in various units are presented in Figure 8. As indicated on the plots, the yaw rate RA^t of the second semitrailer is reduced from 2.7 in the uncontrolled case to 1.7 in the controlled case. The lateral acceleration signals are measured in the centre of gravity of each unit and are displayed in Figure 9. It should again be identified from the plots that the lateral acceleration RA^t of the second semitrailer is reduced from 2.3 to 1.6 by favour of dolly steering.

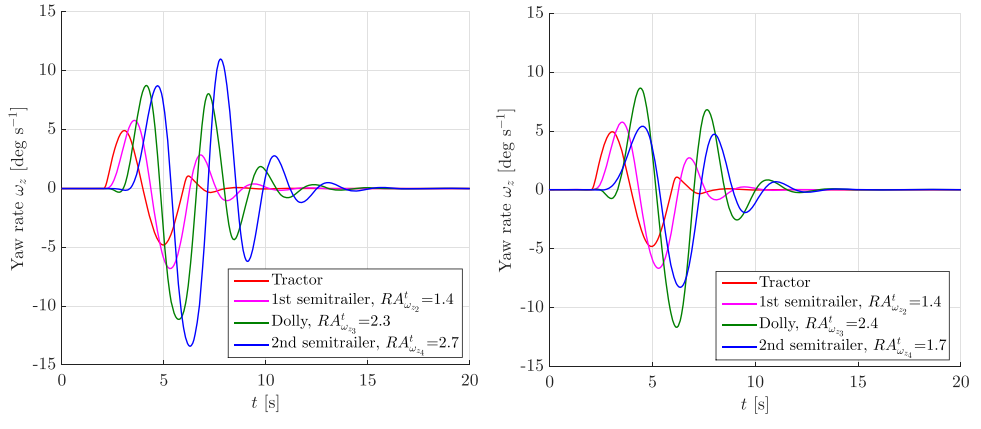

(a) Uncontrolled vehicle (b) Controlled vehicle

Figure 8. Time history of the yaw rate of various units of the A-double in a SLC (v_x = 80 km h^{-1}, driver steering frequency = 0.25 Hz, peak $|a_{y_{11}}|$ = 1.5 m s^{-2})

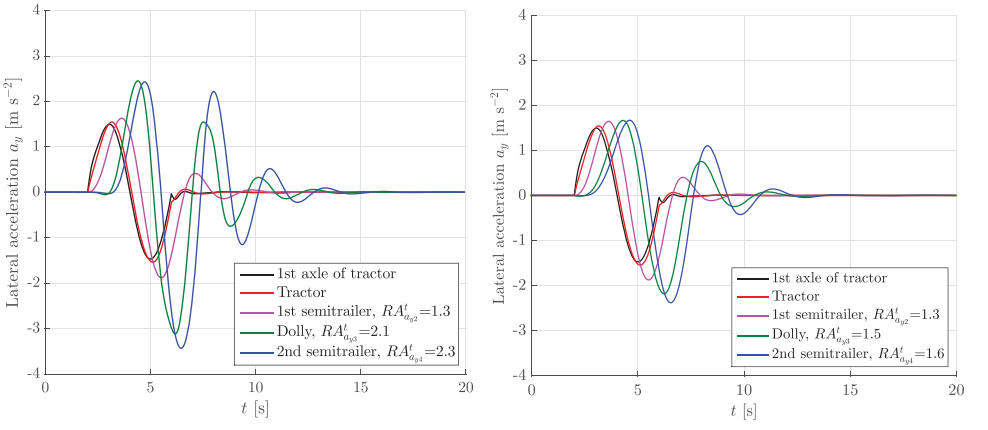

(a) Uncontrolled vehicle (b) Controlled vehicle

Figure 9. Time history of the lateral acceleration of various units of the A-double in an SLC (v_x = 80 km h^{-1}, driver steering frequency = 0.25 Hz, peak $|a_{y_{11}}|$ = 1.5 m s^{-2}).

Another important lateral performance measure is high-speed transient offtracking (HSTO), which is defined as the lateral deviation of the path of the axles in the towed units if compared to the path of the first axle of the tractor (denoted as $axle_{11}$) during an SLC manoeuver. The path of the first axle of the tractor and also the last axles of the other units in this specific SLC manoeuver are depicted in Figure 10. The obtained HSTO values at the centre of axles 6 ($axle_{23}$), 8 ($axle_{32}$), and 11 ($axle_{43}$) of the A-double are also listed in Figure 10. The HSTO in the second semitrailer is reduced from 1.28 to 0.86 m by active dolly steering. A comparative look into Figure 10(a,b) reveals that the trajectory of the controlled vehicle is slightly different from that of the uncontrolled vehicle in the steady-state (with lateral displacements of 4.05 and 4.22 m, respectively). It is thus concluded that the RA suppression and the increased yaw damping ratio caused by the active dolly steering in the controlled vehicle makes its steady-state lateral displacement shorter than that of the

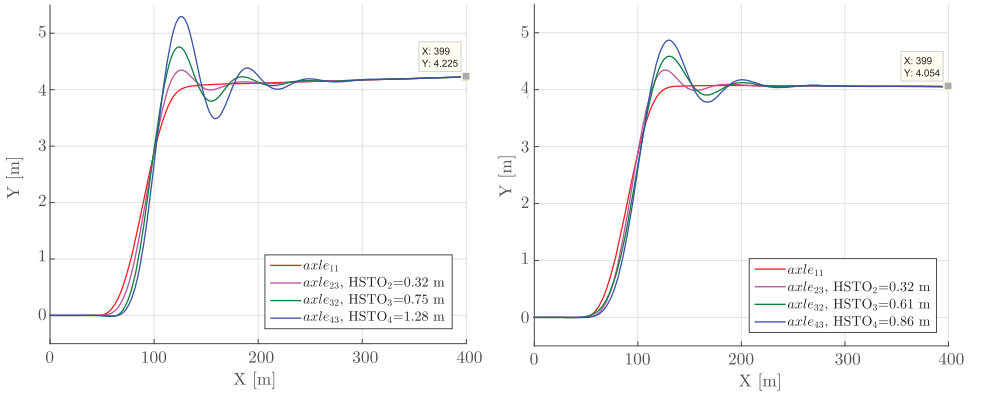

(a) Uncontrolled vehicle (b) Controlled vehicle

Figure 10. Path of the first axle of the tractor and the last axle of the towed units of the A-double in a SLC (v_x = 80 km h^{-1}, driver steering frequency = 0.25 Hz, peak $|a_{y_{11}}|$ = 1.5 m s^{-2})

uncontrolled vehicle in an open loop SLC manoeuver in which there is no corrective driver input [42].

It is thus concluded that the RA^t and HSTO are significantly decreased in the controlled vehicle if compared to the uncontrolled vehicle. In reference to Figure 7, it is observed that this is realised with dolly angles that stay below a peak magnitude of 4.02°.

5. Summary and conclusions

A robust static output-feedback controller is developed for high-speed lateral improvement of the A-double via active steering of the dolly axles. The robust lateral controller is designed by taking into account both the cornering stiffness of the tyres and the moments of inertia of the semitrailers as uncertain vehicle parameters. In order to better capture the nonlinear behaviour of the tyres, a linear time-varying tyre model is used. Moreover to avoid dealing with the system matrices that have rational dependence on the moments of inertia, a descriptor form representation of the linear model is considered. As a result, a time-varying parameter-dependent linear model in descriptor form is achieved to be used in the control synthesis. It is assumed that only measurements of the driver steering input and the articulation angle between the first semitrailer and the dolly are available for feedback. Therefore, a static feedforward is also included in static output feedback formulation as well in order to take into account the driver steering input. Moreover, in order to characterise the frequency content of the driver steering behaviour, a simple bandpass filter is considered as the driver model.

The synthesis procedure is based on LMI optimisation and delivers controllers that ensure robust stability as well as robust performance improvement in the presence of considered parametric uncertainties. This approach requires only the minimum and maximum values of uncertain parameters and also lower and upper bounds on the rates-of-variation of time-varying uncertain parameters. The synthesis is formulated based on $\mathscr{H}_\infty$-type synthesis in which a bound has to be ensured on worst-case energy gains from the driver steering input to the yaw rate of the last semitrailer in order to mitigate the undesired motion amplification in the last semitrailer in response to the driver steering.

As a result, the LMI solvability conditions appear as parameter-dependent LMIs that need to be satisfied over the whole uncertainty range, which leads to infinitely many LMI conditions. To reduce the conservatism, the Lyapunov matrix is chosen to have affine dependence on the uncertain parameters. The multi-convexity approach is employed to achieve finitely many LMI conditions.

The simulation results using both the linear and the high-fidelity vehicle models have shown significant improvement in lateral performance of the A-double in terms of yaw rate and lateral acceleration rearward amplification and high-speed transient offtracking. The controller effectiveness was verified using both time-domain and frequency-domain approaches. As a future task, the controller performance should be further verified in the real environment with a test vehicle.

Acknowledgments

The authors would like to thank the Department of Chassis Strategies and Vehicle Analysis, Volvo Group Trucks Technology and also Niklas Fröjd for providing the authors with the VTM library and their support.

Disclosure statement

No potential conflict of interest was reported by the authors.

Funding

This work was supported by Volvo Technology AB and Strategic Vehicle Research and Innovation [grant number 2017-03036].

ORCID

Maliheh Sadeghi Kati http://orcid.org/0000-0003-3079-4801
Hakan Köroğlu http://orcid.org/0000-0001-5285-7784
Jonas Fredriksson http://orcid.org/0000-0002-9814-6416

References

[1] Kharrazi S. Steering based lateral performance control of long heavy vehicle combinations [PhD thesis]. Gothenburg: Department of Applied Mechanics, Chalmers University of Technology; 2012.
[2] Ding X, Mikaric S, He Y. Design of an active trailer-steering system for multi-trailer articulated heavy vehicles using real-time simulations. Proc Inst Mech Eng Part D: J Automobile Eng. 2013; 227(5):643–655.
[3] Cheng C, Cebon D. Improving roll stability of articulated heavy vehicles using active semi-trailer steering. Vehicle Syst Dyn. 2008;46(sup1):373–388.
[4] Islam MM. Parallel design optimization of multi-trailer articulated heavy vehicles with active safety systems [PhD thesis]. Ontario: University of Ontario Institute of Technology; 2013.
[5] Kim K, Guan H, Wang B, et al. Active steering control strategy for articulated vehicles. Front Inform Technol Electron Eng. 2016;17(6):576–586.
[6] Oreh SHT, Kazemi R, Azadi S. A sliding-mode controller for directional control of articulated heavy vehicles. Proc Inst Mech Eng Part D: J Automobile Eng. 2014;228(3):245–262.
[7] Oehry B, Haas L, van Driel C. Study on heavy vehicle on-board weighing-final report. Basel: Transport & Environment, Rapp Trans AG; December 2013. (Tech. rep.).
[8] Peters B, Koniditsiotis C. Weigh-in-motion technology. Sydney: Austroads Incorporated; 2000. (Tech. Rep. AP-R168/00).
[9] Tai M, Tomizuka M. Robust lateral control of heavy duty vehicles- final report. Berkeley: Institute of Transportation Studies, UC; 2003. (California PATH Research Report UCB-ITS-PRR-2003-24).
[10] Wang JY, Tomizuka M. Robust $\mathcal{H}_\infty$ lateral control of heavy-duty vehicles in automated highway system. Proceedings of the 1999 American Control Conference, Vol. 5, 1999. p. 3671–3675, San Diego, CA, USA.
[11] Meihua T, Tomizuka M. Robust controllers based on feedback linearization for automated lane guidance of heavy vehicles. IFAC Proceedings, Vol. 33, no. 26, 2000. p. 77–82. IFAC Conference on Mechatronic Systems, Darmstadt, Germany.
[12] Mary AD, Mathew AT, Jacob J. A Robust $\mathcal{H}_\infty$ Control Approach of Uncertain Tractor Trailer System. IETE J Res. 2013;59(1):38–47.
[13] Ni Z. Design and validation of high speed active trailer steering system for articulated heavy vehicle. [Master's thesis]. Oshawa: Mechanical Engineering, University of Ontario Institute of Technology; 2016.
[14] Kati MS, Köroğlu H, Fredriksson J. Robust control of an A-double with active dolly based on static output feedback and dynamic feed-forward. International Forum for Road Transport Technology, 15th International Heavy Vehicle Transport Technology Symposium. Roturua; October 2016.

[15] Byrne RH, Abdallah C. Robust lateral control of highway vehicles. Proceedings of the Intelligent Vehicles '94 Symposium. October 1994. p. 375–380, Paris, France.
[16] Jin X, Yin G, Zeng X, et al. Robust gain-scheduled output feedback yaw stability control for in-wheel-motor-driven electric vehicles with external yaw-moment. J Franklin Inst. 2017. doi:10.1016/j.jfranklin.2017.07.006.
[17] Du H, Zhang N, Dong G. Stabilizing vehicle lateral dynamics with considerations of parameter uncertainties and control saturation through robust yaw control. IEEE Trans Vehicular Technol. 2010;59:2593–2597.
[18] Kati MS, Köroğlu H, Fredriksson J, et al. Robust static output feedback with dynamic feedforward for lateral control of long combination vehicles at high speeds. IEEE Trans Control Syst Technol. 2018.
[19] Benton RE, Smith D. A static-output-feedback design procedure for robust emergency lateral control of a highway vehicle. IEEE Trans Control Syst Technol. 2005;13(4):618–623.
[20] Benton RE. Linear matrix inequality approach to robust emergency lateral control of a highway vehicle with time-varying uncertainties [PhD thesis]. Louisiana State University and Agricultural & Mechanical College; 1997.
[21] Jin XJ, Yin G, Chen N. Gain-scheduled robust control for lateral stability of four-wheel-independent-drive electric vehicles via linear parameter-varying technique. Mechatronics. 2015;30:286–296.
[22] Polat I, Eskinat E, Köse IE. Dynamic output feedback control of quasi-LPV mechanical systems. IET Control Theory Appl. 2007;1(4):1114–1121.
[23] Chen C, Tomizuka M. Dynamic modeling of articulated vehicles for automated highway systems. American Control Conference, Proceedings of the 1995. Vol. 1. 1995 Jun. p. 653–657, Seattle, WA, USA.
[24] Levén M, Sjöblom A, Lidberg M. Derivation of linear single-track truck-dolly-semitrailer model with steerable axles. Gothenburg, Sweden: Department of Applied Mechanics, Chalmers University of Technology; 2011. (Tech. rep.).
[25] Nilson P. Traffic situation management for driving automation of articulated heavy road transports, from driver behaviour towards highway autopilot [PhD thesis]. Gothenburg, Sweden: Department of Mechanics and Maritime Science, Chalmers University of Technology; 2017.
[26] Pacejka H. Tire and vehicle dynamics. 3rd ed. Vol. Oxford, UK: Butterworth-Heinemann; 2012.
[27] Sundström P, Laine L. Validation of VTM model of tractor 4x2 with semitrailer using winter test results from arjeplog 2111w11 p2685. Gothenburg, Sweden; 2012. (Tech. rep.).
[28] Westerhof B, Kalakos D. Heavy vehicle braking using friction estimation for controller optimization [Master's thesis]. Gothenburg, Sweden: Department of Applied Mechanics, Chalmers University of Technology; 2017.
[29] Köroğlu H, Falcone P. New LMI conditions for static output feedback synthesis with multiple performance objectives. Proc. 53rd IEEE Conference on Decision and Control. Los Angeles, CA: 2014. p. 866–871.
[30] Kati MS, Köroğlu H, Fredriksson J. $\mathcal{H}_\infty$ static output feedback synthesis under an integral quadratic constraint with application to high capacity transport vehicles. 2016 European Control Conference (ECC). 2016 June. p. 1999–2004, Aalborg, Denmark.
[31] Wei X, Verhaegen M. LMI solutions to the mixed $\mathcal{H}-/\mathcal{H}_\infty$ fault detection observer design for linear parameter-varying systems. Int J Adapt Control Signal Process. 2011;25(2):114–136.
[32] Scherer C. LMI relaxations in robust control. Eur J Control. 2006;12(1):3–29.
[33] Gahinet P, Apkarian P, Chilali M. Affine parameter-dependent Lyapunov functions and real parametric uncertainty. IEEE Trans Automat Contr. 1996;41(3):436–442.
[34] Löfberg J. YALMIP: a toolbox for modeling and optimization in MATLAB. 2004 IEEE International Conference on Robotics and Automation, no. 04CH37508. Taipei, Taiwan; 2004 September. p. 284–289.
[35] Sturm JF. Using SeDuMi 1.02, a Matlab toolbox for optimization over symmetric cones. Optim Methods Softw. 1999;11(1–4):625–653.

[36] Powell R. Relationships between lane change performance and open-loop handling metrics. [Master thesis]. South Carolina, USA: Department of Mechanical Engineering, Clemson University; 2009.
[37] Zhu S, He Y. Articulated heavy vehicle lateral dynamic analysis using an automated frequency response measuring technique. Int J Vehicle Perform. 2015;2(1):30–57.
[38] Aurell J, Winkler CB. Standard test procedures for the lateral stability of heavy vehicle combinations. International Symposium on Heavy Vehicle Weights and Dimensions. 1995. p. 463–471, Ann Arbor, MI, USA.
[39] Swedish Standards Institute. Road vehicles- Heavy commercial vehicle combinations and articulated buses-Lateral stability test methods. Svensk Standard SS-ISO 14791 ICS 43.080.01, Stockholm; 2002.
[40] van de Molengraft-Luijten MFJ, Besselink IJM, Verschuren RMAF, et al. Analysis of the lateral dynamic behaviour of articulated commercial vehicles. Vehicle Syst Dyn. 2012;50(sup1):169–189.
[41] National Transport Commission (NTC). Performance based standards scheme – the standards and vehicle assessment rules, Melbourne, Australia; 2008. (Tech. rep.).
[42] Wang Q, He Y. A study on single lane-change manoeuvres for determining rearward amplification of multi-trailer articulated heavy vehicles with active trailer steering systems. Vehicle Syst Dyn. 2016;54(1):102–123.

Appendix 1: Linear vehicle model parameters

The vehicle parameters used in the linear vehicle model are listed in Table A1.

Table A1. Vehicle model parameters.

Parameter	Description	Value	Unit
m_1	Mass of tractor	9840	kg
m_2	Mass of 1st semitrailer	31,570	kg
m_3	Mass of dolly	3400	kg
m_4	Mass of 2nd semitrailer	33,740	kg
a_1	Distance between COG* and 1st axle of tractor	1.5411	m
a_2	Distance between COG and front coupling point of 1st semitrailer	4.5089	m
a_3	Distance between COG and front coupling point of dolly	4.0847	m
a_4	Distance between COG and front coupling point of 2nd semitrailer	4.2355	m
c_1	Distance between COG and rear coupling point of tractor	2.2339	m
c_2	Distance between COG and rear coupling point of 1st semitrailer	5.8911	m
c_3	Distance between COG and rear coupling point of dolly	0.2253	m
b_1	Distance between COG and centre of rear axles group of tractor	2.5089	m
b_2	Distance between COG and centre of rear axles group of 1st semitrailer	3.1911	m
b_3	Distance between COG and centre of rear axles group of dolly	0.2553	m
b_4	Distance between COG and centre of rear axles group of 2nd semitrailer	3.4645	m
ω_c	Centre frequency of driver model	2.6284	rad s^{-1}
ζ	Damping ratio of driver model	1.9347	

Note: *Represents centre of gravity.

Appendix 2: Linear vehicle model equations

To derive the motion of the vehicle, it is more convenient to transform the velocities in the inertial coordinates to the body fixed system. To this end, the following transformation matrix in $2D$ Euclidean space is performed

$$\mathrm{R}_2(\phi) = \begin{bmatrix} \cos(\phi) & \sin(\phi) \\ -\sin(\phi) & \cos(\phi) \end{bmatrix}.$$

The velocities of different units used in Equation (3) are defined in the corresponding center of gravity of each unit and are obtained as

$$
\begin{aligned}
v_1 &= [v_{x_1}\ v_{y_1}],\\
v_2 &= [v_{x_1}\ v_{y_1} - c_1\omega_{z_1}] + [0\ -a_2\omega_{z_2}]\,\mathrm{R}_2(\theta_1),\\
v_3 &= [v_{x_1}\ v_{y_1} - c_1\omega_{z_1}] + [0\ -l_2\omega_{z_2}]\,\mathrm{R}_2(\theta_1) + [0\ -a_3\omega_{z_3}]\,\mathrm{R}_2(\theta_1+\theta_2),\\
v_4 &= [v_{x_1}\ v_{y_1} - c_1\omega_{z_1}] + [0\ -l_2\omega_{z_2}]\,\mathrm{R}_2(\theta_1) + [0\ -l_3\omega_{z_3}]\,\mathrm{R}_2(\theta_1+\theta_2)\\
&\quad + [0\quad -a_4\omega_{z_4}]\,\mathrm{R}_2(\theta_1+\theta_2+\theta_3),
\end{aligned}
$$

where $l_2 = a_2 + c_2,\ l_3 = a_3 + c_3$. Note that the yaw rates and yaw angles of the three units are expressed in the coordinate system of the first unit ($\omega_{z_1} = \dot{\varphi}_1$) as follows:

$$
\begin{aligned}
&\omega_{z_2} = \omega_{z_1} + \dot{\theta}_1, \quad \omega_{z_3} = \omega_{z_1} + \dot{\theta}_1 + \dot{\theta}_2, \quad \omega_{z_4} = \omega_{z_1} + \dot{\theta}_1 + \dot{\theta}_2 + \dot{\theta}_3,\\
&\varphi_2 = \varphi_1 + \theta_1, \quad \varphi_3 = \varphi_1 + \theta_1 + \theta_2, \quad \varphi_4 = \varphi_1 + \theta_1 + \theta_2 + \theta_3.
\end{aligned}
$$

The tyre forces including the lateral forces and the slip angles in Equation (4) are expressed in the global frame can be written as follows:

$$
\begin{aligned}
&F_{1_f} = [F_{x_{1_f}}\ F_{y_{1_f}}]\mathrm{R}_2(\phi_1 + \delta_{driver}), \quad F_{y_{1_f}} = C_{1_f}\alpha_{1_f}, \quad \alpha_{1_f} = -\arctan\left(\frac{v_{y_{1_f}}}{v_{x_{1_f}}}\right) + \delta_{driver},\\
&F_{1_r} = [F_{x_{1_f}}\ F_{y_{1_r}}]\mathrm{R}_2(\phi_1), \quad F_{y_{1_r}} = C_{1_r}\alpha_{1_r}, \quad \alpha_{1_r} = -\arctan\left(\frac{v_{y_{1_r}}}{v_{x_{1_r}}}\right),\\
&F_2 = [F_{x_2}\ F_{y_2}]\mathrm{R}_2(\phi_2), \quad F_{y_2} = C_2\alpha_2, \quad \alpha_2 = -\arctan\left(\frac{v_{y_{2_t}}}{v_{x_{2_t}}}\right),\\
&F_3 = [F_{x_3}\ F_{y_3}]\mathrm{R}_2(\phi_3 + \delta_{dolly}), \quad F_{y_3} = C_3\alpha_3, \quad \alpha_3 = -\arctan\left(\frac{v_{y_{3_t}}}{v_{x_{3_t}}}\right) + \delta_{dolly},\\
&F_4 = [F_{x_4}\ F_{y_4}]\mathrm{R}_2(\phi_4), \quad F_{y_4} = C_4\alpha_4, \quad \alpha_4 = -\arctan\left(\frac{v_{y_{4_t}}}{v_{x_{4_t}}}\right),
\end{aligned}
$$

Recall that since no braking or acceleration are assumed and a constant longitudinal velocity is considered, longitudinal forces are set equal to zero. The velocities of different axles groups used in the calculation of the slip angles are obtained as the following

$$
\begin{aligned}
v_{1_f} &= [v_{x_{1_f}}\ v_{y_{1_f}}] = [v_{x_1}\ v_{y_1} + a_1\omega_{z_1}]\mathrm{R}_2(\phi_1),\\
v_{1_r} &= [v_{x_{1_r}}\ v_{y_{1_r}}] = [v_{x_1}\ v_{y_1} - b_1\omega_{z_1}]\mathrm{R}_2(\phi_1),\\
v_{2_t} &= [v_{x_{2_t}}\ v_{y_{2_t}}] = [v_{x_1}\ v_{y_1} - c_1\omega_{z_1}]\mathrm{R}_2(\phi_1) + [0\ -(a_2+b_2)\omega_{z_2}]\mathrm{R}_2(\phi_2)\\
v_{3_t} &= [v_{x_{3_t}}\ v_{y_{3_t}}] = [v_{x_1}\ v_{y_1} - c_1\omega_{z_1}]\mathrm{R}_2(\phi_1) + [0\ -l_2\omega_{z_2}]\mathrm{R}_2(\phi_2) + [0\ -(a_3+b_3)\omega_{z_3}]\mathrm{R}_2(\phi_3),\\
v_{4_t} &= [v_{x_{4_t}}\ v_{y_{4_t}}] = [v_{x_1}\ v_{y_1} - c_1\omega_{z_1}]\mathrm{R}_2(\phi_1) + [0\ -l_2\omega_{z_2}]\mathrm{R}_2(\phi_2)\\
&\quad + [0\ -l_3\omega_{z_3}]\mathrm{R}_2(\phi_3) + [0\ -(a_4+b_4)\omega_{z_4}]\mathrm{R}_2(\phi_4),
\end{aligned}
$$

The positions of the tyres used in Equation (4) are expressed in global coordinates and are defined as

$$
\begin{aligned}
r_{1_f} &= \begin{bmatrix} X_1 + a_1\cos(\phi_1) & Y_1 + a_1\sin(\phi_1) \end{bmatrix},\\
r_{1_r} &= \begin{bmatrix} X_1 - b_1\cos(\phi_1) & Y_1 - b_1\sin(\phi_1) \end{bmatrix},\\
r_2 &= \begin{bmatrix} X_1 - c_1\cos(\phi_1) - (a_2+b_2)\cos(\phi_2) & Y_1 - c_1\sin(\phi_1) - (a_2+b_2)\sin(\phi_2) \end{bmatrix},\\
r_3 &= \begin{bmatrix} X_1 - c_1\cos(\phi_1) - l_2\cos(\phi_2) - (a_3+b_3)\cos(\phi_3) \\ Y_1 - c_1\sin(\phi_1) - l_2\sin(\phi_2) - (a_3+b_3)\sin(\phi_3) \end{bmatrix}^T,\\
r_4 &= \begin{bmatrix} X_1 - c_1\cos(\phi_1) - l_2\cos(\phi_2) - l_3\cos(\phi_3) - (a_4+b_4)\cos(\phi_4) \\ Y_1 - c_1\sin(\phi_1) - l_2\sin(\phi_2) - l_3\sin(\phi_3) - (a_4+b_4)\sin(\phi_4) \end{bmatrix}^T,
\end{aligned}
$$

where r_{1_f} and r_{1_f} are the positions of the front axle and the center of the driven axles group, respectively. r_2, r_3 and r_4 are also the center position of the axle groups in the first semitrailer, the dolly and the second semitrailer, respectively. Finally, the matrices $\mathcal{M}_q$, $\mathcal{K}_q$, $\mathcal{C}_q$, $\mathcal{H}_q$ and $\mathcal{B}_q$ are obtained as the following:

$$
\mathcal{M}_q = \begin{bmatrix} M_{11} & M_{12} & M_{13} & M_{14} & M_{15} \\ * & M_{22} & M_{23} & M_{24} & M_{25} \\ * & * & M_{33} & M_{34} & M_{35} \\ * & * & * & M_{44} & M_{45} \\ * & * & * & * & M_{55} \end{bmatrix}, \mathcal{K}_q = \begin{bmatrix} 0 & 0 & K_{13} & K_{14} & K_{15} \\ 0 & 0 & K_{23} & K_{24} & K_{25} \\ 0 & 0 & K_{33} & K_{34} & K_{35} \\ 0 & 0 & K_{43} & K_{44} & K_{45} \\ 0 & 0 & K_{53} & K_{54} & K_{55} \end{bmatrix},
$$

$$
\mathcal{B}_q = -C_4 \begin{bmatrix} -1 \\ (c_1 + l_2 + a_3 + b_3) \\ (l_2 + a_3 + b_3) \\ (a_3 + b_3) \\ 0 \end{bmatrix}, \mathcal{H}_q = C_1 \begin{bmatrix} 1 \\ -a_1 \\ 0 \\ 0 \\ 0 \end{bmatrix}, \mathcal{C}_q = \begin{bmatrix} C_{11} & C_{12} & C_{13} & C_{14} & C_{15} \\ * & C_{22} & C_{23} & C_{24} & C_{25} \\ * & * & C_{33} & C_{34} & C_{35} \\ * & * & * & C_{44} & C_{45} \\ * & * & * & * & C_{55} \end{bmatrix} / v_x
$$

$$
+ \begin{bmatrix} 0 & m_1 + m_2 + m_3 + m_4 & 0 & 0 & 0 \\ 0 & -m_2(c_1 + a_2) - m_3(c_1 + l_2 + a_3) - m_4(c_1 + l_2 + l_3 + a_4) & 0 & 0 & 0 \\ 0 & -m_2 a_2 - m_3(l_2 + a_3) & 0 & 0 & 0 \\ 0 & -m_3 a_3 - m_4(l_3 + a_4) & 0 & 0 & 0 \\ 0 & -m_4 a_4 & 0 & 0 & 0 \end{bmatrix} v_x,
$$

Here $*$'s represent entries that are identifiable from symmetry. The elements of $\mathcal{M}_q$ (represented as M_{ij}):

$$
\begin{aligned}
&M_{11} = m_1 + m_2 + m_3 + m_4,\ M_{12} = -m_2(c_1 + a_2) - m_3(c_1 + l_2 + a_3) - m_4(c_1 + l_2 + l_3 + a_4),\\
&M_{13} = -m_2 a_2 - m_3(l_2 + a_3) - m_4(l_2 + l_3 + a_4),\\
&M_{14} = -m_3 a_3 - m_4(l_3 + a_4), \quad M_{15} = -m_4 a_4,\\
&M_{22} = I_{z_1} + I_{z_2} + I_{z_3} + I_{z_4} + m_2(c_1 + a_2)^2 + m_3(c_1 + l_2 + a_3)^2 + m_4(c_1 + l_2 + l_3 + a_4)^2,\\
&M_{23} = I_{z_2} + I_{z_3} + I_{z_4} + m_2 a_2(c_1 + a_2) + m_3(l_2 + a_3)(c_1 + l_2 + a_3)\\
&\qquad + m_3(l_2 + a_3)(c_1 + l_2 + a_3) + m_4(l_2 + l_3 + a_4)(c_1 + l_2 + l_3 + a_4),\\
&M_{24} = I_{z_3} + I_{z_4} + m_3 a_3(c_1 + l_2 + a_3) + m_4(l_3 + a_4)(c_1 + l_2 + l_3 + a_4),\\
&M_{25} = I_{z_4} + m_4 a_4(c_1 + l_2 + l_3 + a_4),\\
&M_{33} = I_{z_2} + I_{z_3} + I_{z_4} + m_2 a_2^2 + m_3(l_2 + a_3)^2 + m_4(l_2 + l_3 + a_4)^2,\\
&M_{34} = I_{z_3} + I_{z_4} + m_3 a_3(l_2 + a_3) + m_4(l_3 + a_4)(l_2 + l_3 + a_4),
\end{aligned}
$$

$$M_{35} = I_{z_4} + m_4 a_4 (l_2 + l_3 + a_4), \quad M_{44} = I_{z_3} + I_{z_4} + m_3 a_3^2 + m_4 (l_3 + a_4)^2,$$
$$M_{45} = I_{z_4} + m_4 a_4 (l_3 + a_4), \quad M_{55} = I_{z_4} + m_4 a_4^2.$$

The elements of $\mathcal{K}_q$ (represented as K_{ij}):

$$K_{13} = -(C_2 + C_3 + C_4), \quad K_{14} = -(C_3 + C_4), \quad K_{15} = -C_4,$$
$$K_{23} = C_2(c_1 + a_2 + b_2) + C_3(c_1 + l_2 + a_3 + b_3) + C_4(c_1 + l_2 + l_3 + a_4 + b_4),$$
$$K_{24} = C_3(c_1 + l_2 + a_3 + b_3) + C_4(c_1 + l_2 + l_3 + a_4 + b_4), K_{25} = C_4(c_1 + l_2 + l_3 + a_4 + b_4),$$
$$K_{33} = C_2(a_2 + b_2) + C_3(l_2 + a_3 + b_3) + C_4(l_2 + l_3 + a_4 + b_4),$$
$$K_{34} = C_3(l_2 + a_3 + b_3) + C_4(l_2 + l_3 + a_4 + b_4),$$
$$K_{35} = C_4(l_2 + l_3 + a_4 + b_4), K_{43} = C_2 l_3 + C_3(a_3 + b_3 + a_4 + b_4),$$
$$K_{45} = C_4(l_3 + a_4 + b_4), \quad K_{53} = K_{54} = K_{55} = C_4(a_4 + b_4).$$

The elements of $\mathcal{C}_q$ (represented as C_{ij}):

$$C_{11} = C_{1_f} + C_{1_r} + C_2 + C_3 + C_4,$$
$$C_{12} = -C_{1_f} a_1 + C_{1_r} b_1 - C_2(c_1 + l_2) - C_3(c_1 + l_2 + a_3 + b_3) - C_4(c_1 + l_2 + l_3 + a_4 + b_4),$$
$$C_{13} = -C_2(a_2 + b_2) - C_3(l_2 + a_3 + b_3) - C_4(l_2 + l_3 + a_4 + b_4),$$
$$C_{14} = -C_3(a_3 + b_3) - C_4(l_3 + a_4 + b_4), C_{15} = -C_4(a_4 + b_4),$$
$$C_{21} = C_{1_f} a_1 - C_{1_r} b_1 - C_2(c_1 + a_2 + b_2) - C_3(c_1 + l_2 + a_3 + b_3) - C_4(c_1 + l_2 + l_3 + a_4 + b_4),$$
$$C_{22} = C_{1_r} a_1^2 + C_{1_r} b_2^2 + C_2(c_1 + a_2 + b_2)^2 + C_3(c_1 + l_2 + a_3 + b_3)^2$$
$$+ C_4(c_1 + l_2 + l_3 + a_4 + b_4)^2),$$
$$C_{23} = C_2(a_2 + b_2)(a_1 + a_2 + b_2) + C_3(l_2 + a_3 + b_3)(a_1 + l_2 + a_3 + b_3) +$$
$$+ C_4(l_2 + l_3 + a_4 + b_4)(a_1 + l_2 + l_3 + a_4 + b_4),$$
$$C_{24} = C_3(a_3 + b_3)(a_1 + l_2 + a_3 + b_3) + C_4(l_3 + a_4 + b_4)(a_1 + l_2 + l_3 + a_4 + b_4),$$
$$C_{25} = C_4(a_4 + b_4)(a_1 + l_2 + l_3 + a_4 + b_4),$$
$$C_{33} = C_2(a_2 + b_2)^2 + C_3(l_2 + a_3 + b_3)^2 + C_4(l_2 + l_3 + a_4 + b_4)^2,$$
$$C_{34} = C_3(a_3 + b_3)(l_2 + a_3 + b_3) + C_4(l_3 + a_4 + b_4)(l_2 + l_3 + a_4 + b_4),$$
$$C_{35} = C_4(a_4 + b_4)(l_2 + l_3 + a_4 + b_4), C_{44} = C_3(a_3 + b_3)^2 + C_4(l_3 + a_4 + b_4)^2,$$
$$C_{45} = C_4(a_4 + b_4)(l_3 + a_4 + b_4), C_{55} = C_4(a_4 + b_4)^2.$$